2005-01-2411

Improved Estimation of Linear and Nonlinear Hydraulic Mount Models for Transient Responses

Song He and Rajendra Singh
Acoustics and Dynamics Laboratory
The Ohio State University

ABSTRACT

New procedures are proposed to estimate the amplitude-sensitive parameters of hydraulic engine mounts that typically exhibit many nonlinearities. The estimation is based on the premise that the analyst has access to limited dynamic stiffness test data (say up to 50 Hz), and the detailed laboratory work required for the nonlinear model development would be minimized. By using an analogous mechanical model, a $3^{rd}/2^{nd}$ type transfer function is suggested to curve-fit the empirical dynamic stiffness data. Key parameters (such as the inertia-augmented fluid damping and decoupler gap length) are approximated and the effects of some system nonlinearities (such as the vacuum-induced asymmetric chamber compliance) are quantified, leading to a quasi-linear model. For the sake of illustration, transient predictions for a free decoupler mount are made; simulations match well with measurements. Main simplifications and limitations of the method are briefly discussed.

INTRODUCTION

MOUNT NONLINEARITIES

Hydraulic engine mounts usually exhibit the following nonlinearities in most applications: (i) upper chamber compliance $C_1(p_1)$ where p_1 is the fluid pressure, (ii) flow resistances through inertia track (R_i) and decoupler (R_d), (iii) decoupler switching action, and (iv) vacuum phenomenon in the upper chamber [1, 4]. Kim and Singh [2] first proposed experimental methods to characterize some of the nonlinearities. Their work was refined by Tiwari et al. [1]; also, they extended the nonlinear formulation with empirically obtained functions (or curve-fits) to the prediction of responses to ideal transient excitations. Yet another recent article by Geisberger *et al.* [3] has suggested that a detailed experiment must be constructed before the nonlinear model parameters can be adequately estimated. Such experimental approaches are necessary for research studies but they pose significant difficulties for mount manufactures and users (vehicle designers) as they may have tens or even hundreds of mount designs at their disposal and do not have the luxury of time, or even the facility, to fully characterize the parameters. What is ideally needed would be an approach that would employ limited (and off the shelf) information such as measured data in the form of dynamic stiffness spectra $\tilde{K}(f, X)$ up to 50 Hz for certain excitation displacement amplitudes (X, mm). The development of such an approach is the focus of this article.

OBJECTIVES

In our proposed approach, we first assess the following constraints from the perspective of system user or manufacturer: (a) The mount is viewed as a black-box component with very limited information provided by the mount vendors to protect their proprietary designs; (b) Only steady state $\tilde{K}(f, X)$ data are available; (c) An experimental facility to conduct bench tests as suggested by researchers [1-4] is not available; and (d) Time is of essence since the product design cycles are now very stringent. Accordingly we develop new procedures to quickly develop linear and quasi-linear $\tilde{K}(f, X)$ formulations with reasonable accuracy at low frequencies (up to 50 Hz) to quantify the inertia-augmented fluid damping R_i and asymmetric (nonlinear) characteristics of C_1. The effects of amplitude-dependent parameters will also be discussed with focus on quasi-linear models. For the sake of illustration, transient step responses will be predicted in terms of transmitted force and upper chamber pressure using estimated parameters.

DYNAMIC STIFFNESS MEASUREMENTS

All mount vendors and users employ the dynamic stiffness testing procedure, corresponding to the ISO standard 10846 [6]. Commercial machines [7] are readily available though they may not be able to accommodate non-sinusoidal tests. The mount (along with the fixture) is usually placed in an elastomer test machine and a sinusoidal displacement excitation $x(t) = X \cdot \sin(2\pi ft)$

with peak-to-peak (p-p) amplitude X at frequency f is applied, under a compressive preload F_m to produce the mean displacement x_m. The complex-valued, cross point dynamic stiffness $\tilde{K}(f,X) = \left(\left|F_T\right|/X\right)e^{i\phi} = Ke^{i\phi}$ is measured where F_T is the amplitude of force transmitted at f, $K(f,X)$ is the stiffness modulus and $\phi(f,X)$ is the loss angle. In this procedure, a Fourier filter is used to assess response only at f though other frequencies (such as super-harmonics) may be present [1]. Thus, it is difficult to directly quantify the nature and extent of nonlinearities based on the above procedure.

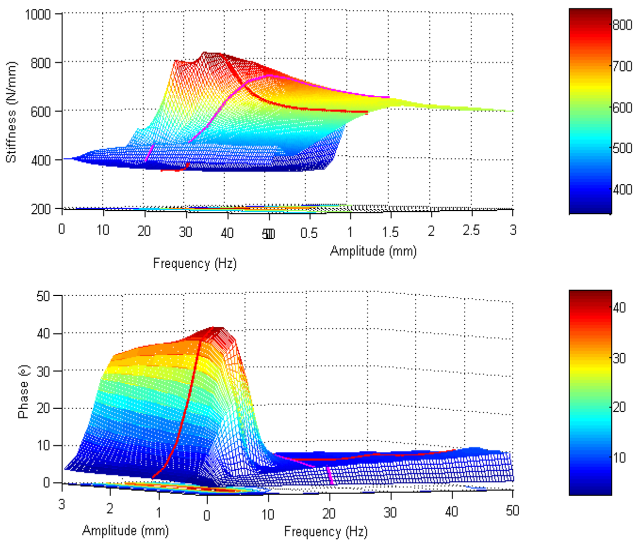

Fig. 1 Surface interpolated $\tilde{K}(f,X)$ data from discrete stiffness measurements

Figure 1 shows one set of $\tilde{K}(f,X)$ 2-D function surface interpolated using the bi-linear method with resolutions Δf = 0.5 Hz and ΔX = 0.02 mm. It is based on discrete measurements conducted up to 50 Hz with an increment of 2.5 Hz, corresponding to X values measured at 14 values between 0.1 and 3 mm. Results are plotted in a 3-D form with horizontal axes representing f and X respectively. Thus, various operational conditions could be estimated at intermediate points interpolated from measurements. Other interpolation methods include cubic spline and bi-cubic surface fit, etc [8].

MATHEMATICAL MODEL

LUMPED FLUID MODEL

The hydraulic mount is usually modeled by lumping the fluid system into several control volumes as shown in Figure 2 [4-5]. System parameters include the top (#1) and bottom (#2) fluid chamber compliances C_1 and C_2, elastomeric element (r) stiffness k_r and viscous damping b_r, inertia track inertance I_i, decoupler inertance I_d, fluid resistance R_i, and decoupler resistance R_d.

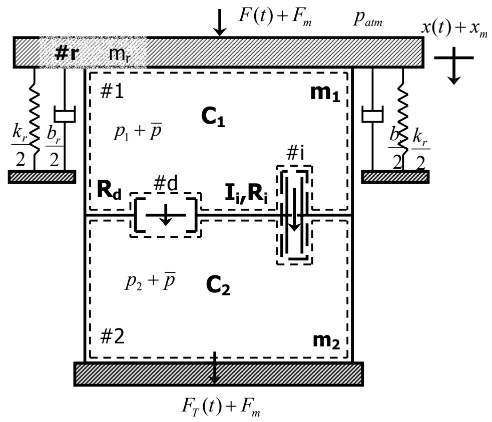

Fig. 2 Lumped fluid model of a generic hydraulic engine mount

We will be using both fluid system parameters (such as C_1 in pressure and volume units) and mechanical system parameters (such as k in force and displacement units). Refer to Singh *et al.* [5] for details. Continuity equations for the bottom and upper chambers of Figure 2 yield the following equations where q_i and q_d are the flow rates through the inertia track and decoupler respectively, A_r is the effective piston area, and p_1 and p_2 are dynamic pressures in top and bottom chambers respectively.

$$A_r\dot{x}(t) - q_i(t) - q_d(t) = C_1\dot{p}_1(t) \tag{1a}$$

$$q_i(t) + q_d(t) = C_2\dot{p}_2(t) \tag{1b}$$

Momentum equations for the decoupler and inertia track are derived as:

$$p_1(t) - p_2(t) = I_d\dot{q}_d(t) + R_d q_d(t) \tag{2a}$$

$$p_1(t) - p_2(t) = I_i\dot{q}_i(t) + R_i q_i(t) \tag{2b}$$

The thin rubber membrane that forms the lower fluid chamber (#2) has a very high compliance C_2 (or low stiffness). Thus the lower chamber (absolute) pressure p_2^t and the static equilibrium pressure $\bar{p}$ can be approximated by the atmosphere pressure p_{atm}. Therefore, the dynamic pressure $p_2(t) = p_2^t - \bar{p} \approx 0$ can be ignored for the sake of simplification. Measured results [1, 2, 4] also confirm that p_2 is negligible compared with p_1, i.e. $p_1(t) - p_2(t) \approx p_1(t)$.

CROSS VS. DRIVING POINT STIFFNESS EXPRESSIONS

The cross point (transfer) dynamic stiffness is given by the dynamic force $F_T(t)$ transmitted to the rigid base that is shown in Figure 2, where F_m is the static force, $F_T^t(t)$ is the absolute force and $p_1(t) = p_1^t(t) - \bar{p}$.

$$F_T^t(t) = F_m + F_T(t) \tag{3a}$$

$$F_m = k_r x_m + A_r(\bar{p} - p_{atm}) \tag{3b}$$

$$F_T(t) = k_r x(t) + b_r \dot{x}(t) + A_r p_1(t) \quad (3c)$$

Suppose we were to apply a dynamic force $F(t)$ at the driving point and evaluate response $x(t)$. This would give us the driving point dynamic stiffness. The effective (but fictitious) dynamic force at the driving point $F(t)$ can be viewed by rewriting (3a-c) as:

$$F^t(t) = F_m + F(t) \quad (3d)$$

$$F(t) = m_r \ddot{x}(t) + k_r x(t) + b_r \dot{x}(t) + A_r p_1(t) \quad (3e)$$

By comparing $F_T(t)$ of (3c) with $F(t)$ of (3e):

$$F(t) = F_T(t) + m_r \ddot{x}(t) \quad (3f)$$

Observe that F(t) includes the additional inertia term corresponding to the rubber element mass m_r. However, $m_r \ddot{x}(t)$ is negligible at lower frequencies due to a small value of m_r. This implies that $F(t) \approx F_T(t)$ and $F / X(f) \approx F_T / X(f)$. This is one of the key assumptions of our estimation method. Experimental work of Lee *et al.* [9] confirms that the driving and cross point dynamic stiffnesses at low frequency regime are virtually the same for most mounts.

ANALOGOUS MECHANICAL MODEL OF THE FIXED DECOUPLER MOUNT

The fixed decoupler type mount can be analyzed as a sub-set of the complete system by inserting $q_d \to 0$ or $R_d \to \infty$. Define the effective parameters of the analogous mechanical system (of Figure 3) as: effective velocity of the inertia track fluid $\dot{x}_{ie}(t) = q_i(t)/A_r$; effective mass of the inertia track fluid column $m_{ie} = A_r^2 I_i$; effective viscous damping of the inertia track fluid $b_{ie} = A_r^2 R_i$; equivalent stiffness of the upper chamber compliance $k_1 = A_r^2 / C_1$; equivalent stiffness of the lower chamber compliance $k_2 = A_r^2 / C_2$.

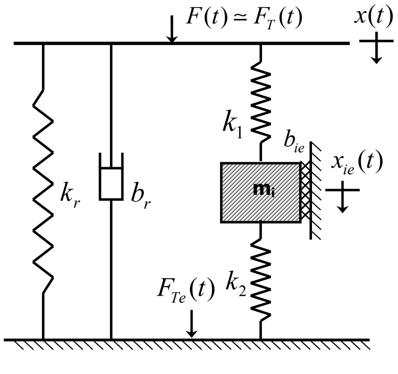

Fig. 3 Analogous mechanical system for a fixed decoupler mount assuming a dynamic force excitation F(t).

From (1) and (2), we get:

$$\dot{p}_2(t) A_r = k_2 \dot{x}_{ie}(t), \quad p_2(t) A_r = k_2 x_{ie}(t) \quad (4a,b)$$

$$\dot{p}_1(t) A_r = k_1 \left[\dot{x}(t) - \dot{x}_{ie}(t) \right] \quad (4c)$$

$$p_1(t) A_r = k_1 \left[x(t) - x_{ie}(t) \right] = F_1(t) \quad (4d)$$

The dynamic force at the driving point is given by

$$F(t) = m_r \ddot{x}(t) + k_r x(t) + b_r \dot{x}(t) + k_1 [x(t) - x_{ie}(t)] \quad (5)$$

The effective governing equation for the inertia track:

$$m_{ie} \ddot{x}_{ie}(t) + b_{ie} \dot{x}_{ie}(t) = k_1 [x(t) - x_{ie}(t)] - k_2 x_{ie}(t) \quad (6)$$

Note that (4b) and (4d) are necessary conditions of (4a) and (4c) respectively so that a numerical error in terms of the mean (dc) components is introduced accordingly. However, this error is found to be trivial for sinusoidal responses.

Table1. Inertia augmented parameters of an effective mechanical model. Here A_i is the effective inertia track area.

Parameter	Physical value	Effective value (in mechanical system units)	Amplification ratio
Inertia track fluid mass	$m_i = A_i^2 I_i$	$m_{ie} = A_r^2 I_i$	A_r^2 / A_i^2
Inertia track damping	$b_i = A_i^2 R_i$	$b_{ie} = A_r^2 R_i$	A_r^2 / A_i^2
Upper chamber stiffness	---	$k_1 = A_r^2 / C_1$	---
Lower chamber stiffness	---	$k_2 = A_r^2 / C_2$	---

Table 1 shows that the effective mass and viscous damping of the fluid inside the inertia track increase proportionally to the square of the area ratio. The reason is that the velocity of the fluid inside the orifice (as well as the force) that accelerates the fluid column is amplified in proportion to the specific cross-sectional area. Therefore, the effective fluid mass of the inertia m_{ie} is of the same order of magnitude as the engine mass m_E (corresponding to the quarter car model [5]), and the resulting hydraulic mount is highly damped when compared with a conventional rubber mount. This mechanism has been referred to as the “velocity amplifying dynamic damper” effect by Sugino *et al.* [10] or “inertia-augmented damping” phenomenon by Singh *et al.* [5].

Assume m_r = 0 over the low frequency regime and transform equations (5, 6) into the Laplace (s) domain where $s = j2\pi f$ and $j = \sqrt{-1}$ (with zero initial conditions). The following driving point dynamic stiffness

(K_{m32}) is obtained in the 3rd/2nd order form corresponding to the mechanical model of Figure 3.

$$K_{m32}(s) = k_r + k_1 + b_r s - \frac{k_1^2}{m_{ie}s^2 + b_{ie}s + k_1 + k_2} \quad (7a)$$

The corresponding static stiffness is derived as $\gamma = k_r + k_1 k_2 / (k_1 + k_2)$. Further, assume $C_2 > 100C_1$ so that $k_1 + k_2 \approx k_1$. Simplify K_{m32} to yield the following expression:

$$K_{m32}(s) = k_r + k_1 + b_r s - \frac{k_1^2}{m_{ie}s^2 + b_{ie}s + k_1} \quad (7b)$$

The denominator polynomial $s^2 + 2\zeta_2\omega_{n2}s + \omega_{n2}^2$ can be converted into $s^2 + (b_{ie}/m_{ie})s + k_1/(m_{ie})$, which implies that ω_{n2} is the natural frequency (in rad/s) of a fluid Helmholtz resonator with compliance C_1 and inertance I_1.

SCOPE AND LIMITATIONS OF THE MECHANICAL MODEL

Rewrite the transmitted force F_T expression as follows using (3e), (2a) and (3f) for the fixed decoupler ($R_d = 0$)

$$F_T(t) = k_r x(t) + b_r \dot{x}(t) + A_r I_i \dot{q}_i(t) + A_r R_i q_i(t) \approx F(t) \quad (8a)$$

Thus F_T has three major components: (i) $k_r x(t) + b_r \dot{x}(t)$ corresponding to the forces transmitted via the rubber element, as represented by the Voight model; (ii) inertia force of the fluid column $A_r I_i \dot{q}(t)$ that can be equated to $m_{ie}\ddot{x}_{ie}(t)$ for the model of Figure 3, and (iii) viscous damping force generated in the inertia track $A_r R_i q_i(t)$ that could be represented by $b_{ie}\dot{x}_{ie}$. Thus, use the mechanical model defined earlier to express $F_T(t)$ as:

$$F_T(t) = k_r x(t) + b_r \dot{x}(t) + m_{ie}\ddot{x}_{ie}(t) + b_{ie}\dot{x}_{ie} \quad (8b)$$

However, from the schematic of mechanical model of Figure 3, the effective transmitted force F_{Te} is found as:

$$\begin{aligned} F_{Te}(t) &= k_r x(t) + b_r \dot{x}(t) + k_2 x_{ie} + b_{ie}\dot{x}_{ie} \\ &\approx k_r x(t) + b_r \dot{x}(t) + b_{ie}\dot{x}_{ie} \end{aligned} \quad (9a)$$

$$F_{Te}(t) = k_r x(t) + b_r \dot{x}(t) + A_r R_i q_i(t) \quad (9b)$$

Comparison of equations (8) and (9) clearly shows that F_{Te} tends to under-estimate F_T by neglecting the inertia force of the inertia track fluid column which is transmitted through the frame. In other words, the dynamic forces (inertia and damping forces) caused by the pressure difference (p_1–p_2) are directly transmitted to the vehicle frame in the fluid model, but only the damping force is transmitted to the fixed base in the mechanical model. Nonetheless, the simplified method can still be used by approximating the driving point dynamic stiffness of the mechanical model as the cross point dynamic stiffness of the fluid model over the low frequency regime. This would allow us to estimate parameters from the K_{m32} transfer function.

ESTIMATION OF AMPLITUDE-DEPENDENT PARAMETERS

FIXED DECOUPLER MOUNT

Using the curve-fitted $\tilde{K}(f, X)$ over the low frequency range (such as Figure 1), a continuous transfer function (in the s domain) is estimated in the 3rd/2nd order form.

$$K_{32}(s) = \frac{n_3 s^3 + n_2 s^2 + n_1 s + n_0}{d_2 s^2 + d_1 s + d_0} \quad (10)$$

Comparison of equations (7b) and (10) shows that d_2, d_1 and d_0 are proportional to m_{ie}, b_{ie} and k_1 respectively. Define a scaling factor δ_0 and assume the static stiffness $\gamma = k_r + k_1 k_2/(k_1 + k_2) \approx k_r + k_2 \approx k_r$. Now, we estimate the system parameters as:

$$k_r = \frac{n_0}{d_0}, \quad b_r = \frac{n_3}{d_2}, \quad \delta_0 = \frac{d_0}{\left(\frac{n_2}{d_0} - b_r \frac{d_1}{d_0}\right)\frac{d_0}{d_2} - k_r}$$

$$k_1 = \frac{d_0}{\delta_0 \varepsilon}, \quad b_{ie} = \frac{d_1}{\delta_0 \varepsilon}, \quad m_{ie} = \frac{d_2}{\delta_0 \varepsilon} \quad (11a\text{-}f)$$

Here ε is a device-specific adjustment ratio (around 1) which could be used to tune δ_0 for best possible curve-fit results. For instance, the value of ε for mount D (Table 2) is found to be around 1.16. Effective parameters are estimated from measured data for the fixed decoupler mount under varying X. Amplitude-dependent results are listed in Table 2 and compared with nominal values (in mechanical system units).

Table 2. Estimated parameters of a fixed decoupler mount D. Baseline values: k_r = 432 N/mm, b_r = 270 Ns/m, $C_1 = 2.5\times10^{-11}$ m^5/N, $R_i = 1.4\times10^{8}$ Ns/m^5, $A_r = 3.31\times10^{-3}$ m^2.

Parameters	Ref.	X (mm) p-p						
Symbols	value	0.3	0.5	1.0	1.5	2.0	2.5	3.0
k_{rm} (N/mm)	432	462	454	439	428	420	414	408
k_r (N/mm)	432	528	535	534	513	494	475	468
b_r (Ns/m)	270	295	282	222	198	186	172	160
k_1 (N/mm)	438	726	610	459	376	319	281	246
b_{ie} (Ns/m)	1534	2056	1964	2018	1971	1921	1923	1872
m_{ie} (kg)	30.8	46.3	45.6	47.0	46.5	45.9	45.9	46.3

Figure 4 shows that predicted $\tilde{K}(f, X)$ spectra using the mechanical model with estimated parameters correlate well with measurements. The nominal chamber stiffnesses satisfy the assumption: $k_2 = 4.6$ N/mm << $k_1 = 438$ N/mm. In Table 2, k_{rm} is the measured value for the rubber element obtained by draining the fluid out of the hydraulic mount. Since both k_{rm} and b_r vary slightly with f, the measured rubber mount data are averaged over the low frequency regime.

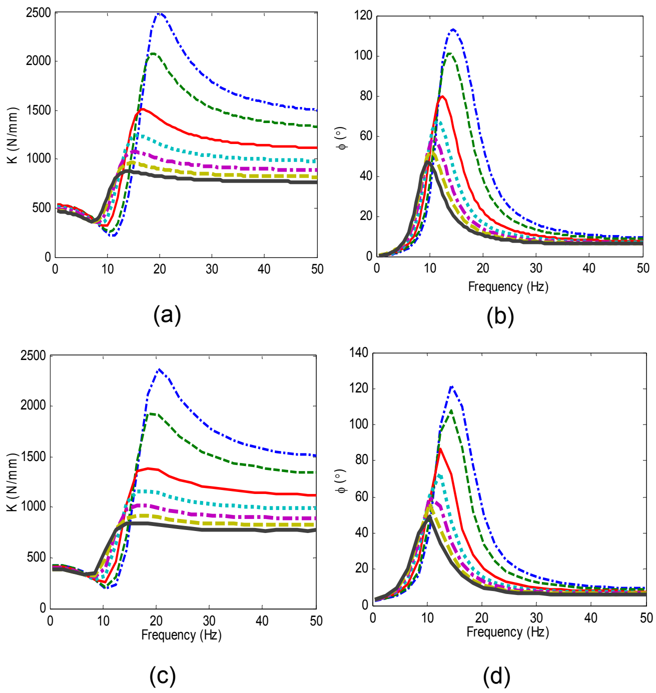

Fig. 4 Dynamic stiffness of a fixed decoupler mount. Measurements are in (a), (c); and (b), (d) show K_{32} predictions. Key: From top to bottom (p-p) X = 0.3, 0.5, 1.0, 1.5, 2, 2.5, 3 mm.

Observe the following interesting results from Table 2: First, both k_{rm} and k_r decrease with an increase in X from 0.3 mm to 3 mm, implying a softening effect in the rubber element under increased amplitude. For a specific X, the value of k_r is approximately 14% higher that that of k_{rm}. This can be explained in terms of the additional stiffness that is introduced by the fluid under an increased static pressure. Therefore, the value of k_r should be regarded as an upper boundary of k_{rm}.

Second, the estimated b_r value decreases slightly with an increase in X even though the measured rubber damping values are almost independent of X. The nominal value can thus be regarded as an averaged value with a ±30% error bound.

Third, estimated m_{ie} values are consistent with each other. As predicted by the mechanical model, m_{ie} is around 46 kg, which is about 1/3 or 1/4 of the engine mass (for a quarter car model) depending on the mounting system. This value is, however, 50% larger than the calculated nominal value. Recall that the inertia track is modeled in our formulation as a straight pipe without any end corrections [4]; thus the effective value elongates the geometric length by up to 33% [11]. Therefore, it is implied that some turbulence takes place within the inertia track [11].

Fourth, similar to the m_{ie} value, the estimated fluid damping b_{ie} is nearly independent of X though it overestimates the measured result by roughly 23%. Since m_{ie}, b_{ie} and k_1 are proportional to the coefficients of the characteristic equation, this error is partially introduced by an over-estimation of m_{ie}. This result also quantifies the inertia augmented damping, and thus b_{ie} is 6 to 10 times more significant than the pure rubber damping b_r.

Finally, many hydraulic mount formulations [3, 10, 13] assume that the amplitude-dependent dynamic stiffness is due to the decoupler action. This assumption implies that the dynamic properties of a fixed decoupler mount will be insensitive to X. However, such is not found in the measured data of Figure 1. Amplitude dependency is illustrated in Table 2 by the estimated k_1, and its value at X = 0.3 mm is nearly three times as the value obtained at X = 3 mm. This difference could be explained by the vacuum phenomenon [1, 2], which is associated with the release of pre-dissolved gas in the fluid during the expansion process. It introduces an additional compliance to the upper chamber. Also, vacuum is more dominant at higher X, resulting in a more significant decrease in the estimated k_1 value. A bi-linear $C_1(p_1)$ model was suggested by Kim and Singh [2] and then Tiwari *et al.* [1, 4] and the $\Delta p_1 / \Delta V_1$ relationship was measured from a bench experiment. As a simplification in our work, a quasi-linear model is proposed where k_1 is modeled as an empirical function of X based on the estimated effective parameters. Then, the following non-linear model is utilized to describe the frequency-sensitive and amplitude-dependent dynamic stiffness of a fixed decoupler mount. For the sake of simplicity, all parameters are assumed to be constants other than the $k_1(X)$ function, which could be interpolated by varying X in a continuous manner.

$$K_{q32}(s,X) = b_r s + k_r + k_1(X) - \frac{k_1^2(X)}{m_{ie}s^2 + b_{ie}s + k_1(X)} \qquad (12)$$

FREE DECOUPLER MOUNT

Next consider the free (or floating) decoupler mount ($R_d \neq 0$ or $q_d \neq 0$) of Figure 2. When the mount is subject to an excitation with higher X, the decoupler remains closed most of the time and the resonance induced by inertia track typically dominates over the low frequency regime. Consequently the governing system should dynamically behave similar to a fixed decoupler mount at lower f. Thus the fixed decoupler mount algorithm could be used to reasonably curve-fit $\tilde{K}(f, X)$ spectra at lower f, provided the estimated parameters are viewed as a consequence of the linearization of all non-linear phenomena including the decoupler switching mechanism, vacuum effect and turbulence. Figure 5 shows sample results for a free decoupler mount where the predicted stiffness spectra correlate well with measurements for $X \geq 1.0$ mm.

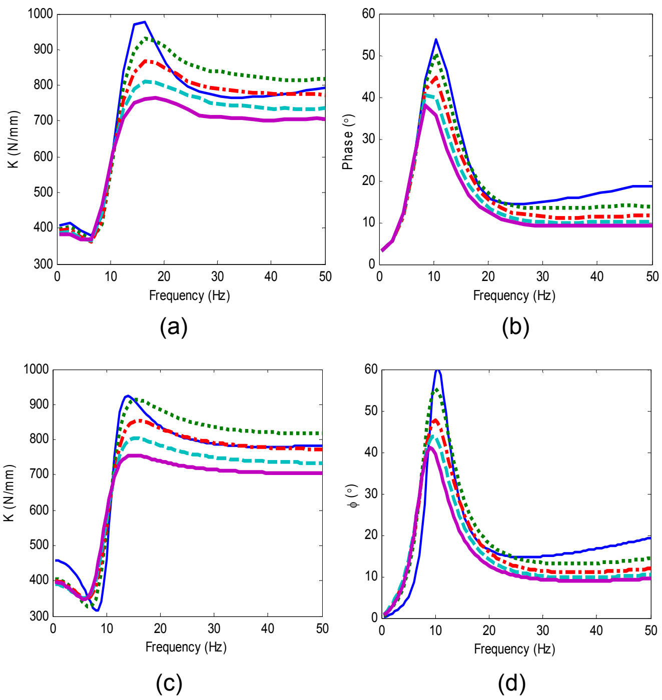

Fig. 5 Dynamic stiffness of a free decoupler mount. Measurements are in (a), (c); and (b), (d) show K_{32} predictions. Key: From top to bottom (p-p): X = 1.0, 1.5, 2, 2.5, 3 mm.

Results are summarized in Table 3, where the estimated parameters for $X \geq 1.5$ mm are found to be consistent with each other.

Table 3. Estimated parameters of a free decoupler mount. Baseline values: k_r = 432 N/mm, b_r = 270 Ns/m, $C_1 = 2.5\times10^{-11}$ m^5/N, $A_r = 3.31\times10^{-3}$ m^2.

Parameters	Nominal	X (mm) p-p				
Symbols	value	1.0	1.5	2.0	2.5	3.0
k_{rm} (N/mm)	432	439	428	420	414	408
k_r (N/mm)	432	458	406.5	400	391	397
b_r (Ns/m)	270	715	480	372	306	259
k_1 (N/mm)	438	233	320	296	376	250
b_{ie} (Ns/m)	1534	1317	2600	2617	2625	2582
m_{ie} (kg)	30.8	37.8	50.8	47.9	48.0	50.3

Abrupt changes are observed in Table 3 when X increases from 1.0 to 1.5 mm, which exhibits a significant increase in b_{ie} from 1317 to 2600 N/m. This implies a shift in the operational state. The inertia track is partially coupled ($q_d \neq 0$) under $X = 1.0$ mm, but it is totally coupled ($q_d = 0$) under $X \geq 1.5$ mm. Assume that the inertia track flow q_i is uncoupled up to a specific excitation amplitude X_d. The decoupler gap length g_d is geometrically related to this X_d by $g_d = \eta X_d A_r / A_d$ where $\eta \leq 1$ is a factor that would account for several effects including the fluid accommodated by the upper chamber and leakage flow through the inertia track. From the results of Table 3, it is inferred that $1.0 \leq X_d \leq 1.5$ mm. Given $A_r = 3.31\times10^{-3}\,\mathrm{m}^2$, $\eta \approx 0.6$ and $A_d = 1.96\times10^{-3}\,\mathrm{m}^2$, the decoupler gap length is estimated as $1.01 \leq g_d \leq 1.51$ mm, which could be further narrowed down by acquiring additional $\tilde{K}(f, X)$ measurements. A careful comparison between simulated and measured $\tilde{K}(f, X)$ spectra yields the value of g_d = 1.1 mm.

When X is 1.5 mm or higher, the estimated k_r, b_r and m_{ie} vary slightly with X and their values are comparable to those of the fixed decoupler mount. Nevertheless, the estimated b_{ie} is higher than the value found for a fixed decoupler by roughly 30%. This strongly suggests that the decoupler switching mechanism introduces additional damping to the inertia augmented fluid damping. Further, the effective k_1 varies with X, which could also be explained by the vacuum effects [1, 2]. This variation, however, is not as significant as the one observed for the fixed decoupler mount. This implies that the decoupler switching mechanism alleviates the softening effect introduced by the vacuum formation (during the expansion process).

VOIGHT VISCO-ELASTIC MODEL PARAMETERS OF THE DECOUPLED MOUNT

For a free decoupler mount, when X is small enough so that the decoupler stays open, the fluid flows essentially through the decoupler gap and the inertia track is completely “decoupled”. In this case, the rubber stiffness and damping tend to dictate dynamic properties. The magnitude spectrum of $\tilde{K}(f, X)$ is relatively flat since the inertia track resonance over the low frequency regime is absent. The Voight visco-elastic model is used to curve-fit the $\tilde{K}(f, X)$ data typically up to 50 Hz in terms of effective spring (k_v) and damper (b_v) that are in parallel as shown in Figure 6.

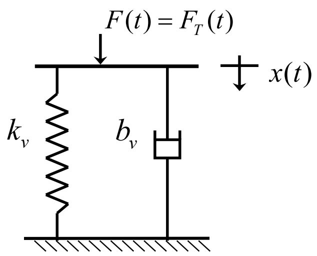

Fig. 6 Voight visco-elastic model at lower *f* when the inertia track is completely decoupled.

The dynamic stiffness of the Voight model is given by $\tilde{K}(f,X) = k_v + j2\pi f \cdot b_v$, where both k_v and b_v weakly depend on *f* and *X*. Using the measured $\tilde{K}(f,X)$ data, mount parameters are estimated in Table 4 corresponding to $X < 1.0$ mm. Alternately, we can curve fit any measured $\tilde{K}(f,X)$ spectra simply by assuming the Voight model but this may not provide any physical interpretation.

Table 4. Estimated parameters of a free decoupler mount using the Voight visco-elastic model.

Parameters	*X* (mm) p-p	
Symbols	0.3	0.5
k_v (N/mm)	468	485
b_v (Ns/m)	338	557

Figure 7 compares the measurement with the Voight model with parameters k_v and b_v. Several "irregular" peaks are observed in measured $\tilde{K}$ at *X* = 0.5, which implies that the mount undergoes a transition between the "decoupled" and "coupled" conditions.

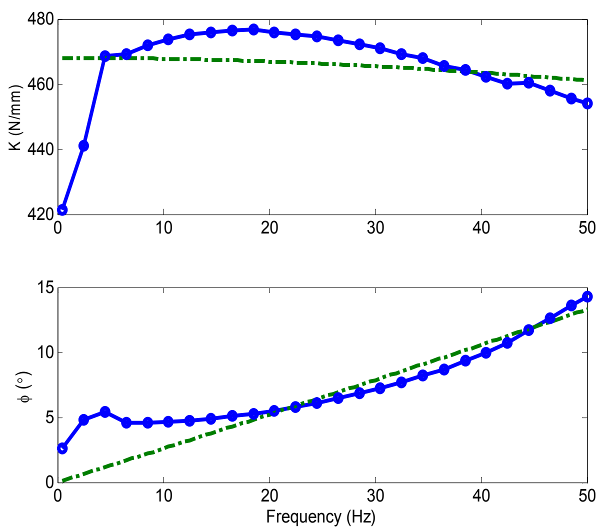

(a)

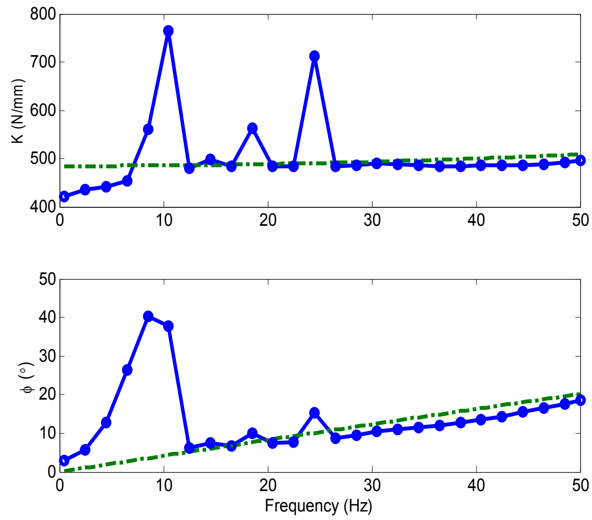

(b)

Fig. 7 $\tilde{K}(f,X)$ results of a free decoupler mount with (a) *X* = 0.3 mm and (b) *X* = 0.5 mm. Key: — measured spectra, ---- curve-fit result using the Voight visco-elastic model.

COMPARISON WITH OTHER ESTIMATION SCHEMES

A brief discussion of prior estimation methods based on measured $\tilde{K}(f,X)$ is as follows. Jeong and Singh [12] utilized the measured $\tilde{K}(f,X)$ data to develop a mount model by employing a nonlinear synthesis method. This resulted in a nonlinear time domain model that was based on a linear model with frequency-dependent parameters. Several empirical functions were defined to characterize the amplitude-dependent properties. However, the coefficients of the dynamic transfer function were numerical values without clearly defined physical significance. Also, such values are obtained by observing the effects of parametric variations on the dynamic stiffness. In our work, we overcome these limitations by determining and utilizing effective mechanical parameters (such as k_1) that can be directly related to the system working principles (such as the vacuum phenomenon) and mount design concepts. Tsujiuchi *et al.* [13] estimated the compliances of C_1 and C_2 by using the measured dynamic characteristics. However, they assumed that the inertia track dimensions are known at the design stage; also, they did not consider the decoupler-induced resonance or damping.

STEP RESPONSES BASED ON MECHANICAL MODEL

DERIVATION OF TRANSFER FUNCTION P_1/X

In order to examine the vacuum effect in the upper chamber, it is desirable to derive the pressure step response $p_{1S}(t)$ and compare it with measurements. A two-stage strategy is applied here. First, the effective parameters are estimated from the curve-fitted K_{32} model as listed in Tables 2 and 3. Second, by assuming that $k_1 >> k_2$ or $k_1 + k_2 \approx k_1$, a simplified $P_1/X(s)$ transfer function is derived as follows. From (6) we obtain:

$$m_{ie}\ddot{x}_{ie}(t) + b_{ie}\dot{x}_{ie}(t) = k_1[x(t) - x_{ie}(t)] \qquad (13)$$

Converting (13) and (4c) into the Laplace domain (s) yields the simplified transfer function as:

$$\frac{P_1}{X}(s) = \frac{k_1}{A_r} \cdot \frac{m_{ie}s^2 + b_{ie}s}{m_{ie}s^2 + b_{ie}s + 1} \qquad (14)$$

It is seen that a constant term is not present in the numerator polynomial so that the static term of (14) is 0 at ω = 0 due to the assumption $C_2 = \infty$ or $1/C_2 = 0$. Note that A_r could be provided by manufacturer or estimated from the cross-section area of the mount and all other parameters are estimated from measured $\tilde{K}(f, X)$ data.

TRANSIENT RESPONSES GIVEN STEP INPUT

The quasi-linear model corresponding to equations (12) and (14) is now used to predict the transient responses. A step-like displacement excitation (Figure 8) is experimentally (and numerically in models) applied to both fixed and free decoupler mounts by releasing the compressive preload from -3.7 mm to -1.32 mm. Here the positive x direction is upward (and negative downward) since that was the convention adopted in the experimental setup [1].

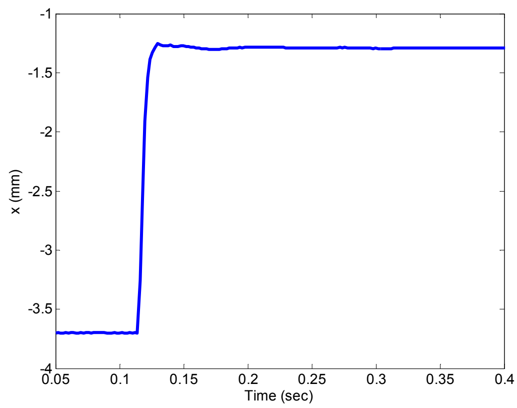

Fig. 8 Measured step-like displacement excitation x(t) from -3.7 to -1.32 mm.

Expressions for $F_T(t)$ and $p_1(t)$ are numerically simulated using the Runge-Kutta 4-5th order algorithm, based on the K_{32} and P_1/X transfer functions and given the step-like excitation of Figure 8. Further, analytical solutions can also be derived in terms of the estimated parameters. (Such details will be given in a future article [14]).

Figures 9 and 10 compare the numerical (time domain solution of the quasi-linear model given the step-like displacement excitation of Figure 8) and analytical solutions (corresponding to an ideal step excitation [14]) for the fixed and free decoupler mounts respectively. The measured time history is represented in Figure 8. Note that the following sign regulations are applied in order to be consistent with measurement data: Negative values of force in Figures 9 and 10 correspond to compressive forces. Likewise, negative value of the dynamic pressure represents a reduction in the value from the reference or mean pressure.

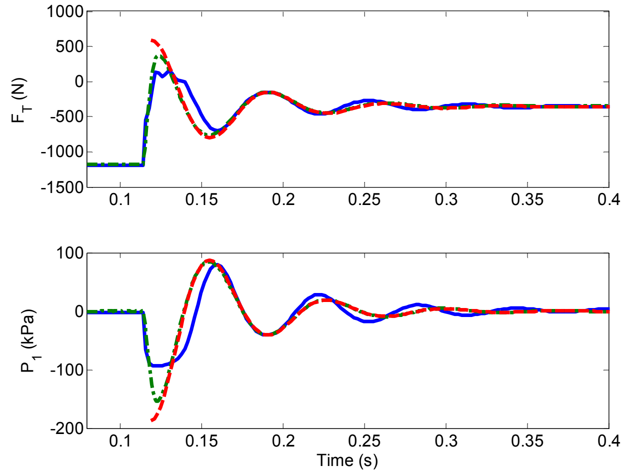

Fig. 9 Step responses for a fixed decoupler mount.
Key: — Measurement given excitation of Fig. 8, -·-· Numerical simulation based on the quasi-linear model (with X = 1.5 mm and excitation of Fig. 8), - - - Analytical solution assuming an ideal step input [14].

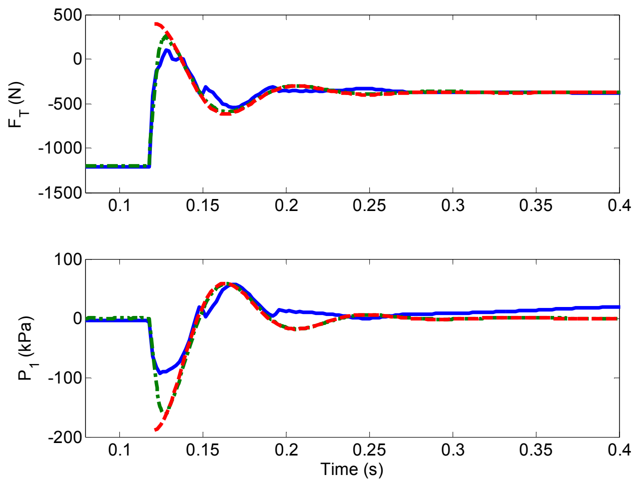

Fig. 10 Step responses for a free decoupler mount.
Key: — Measurement given excitation of Fig. 8, -·-· Numerical simulation based on quasi-linear model (with X = 2 mm and given excitation of Fig. 8), - - - Analytical solution assuming an ideal step input [14].

Due to a finite rise time of the realistic step-like input, slight discrepancies between models and measurements are observed during the initial stages. During the subsequent transient responses, numerical and analytical predictions match well. A flat region in measured curve is, however, found around the first overshoot which may be explained by the vacuum nonlinearity. Best predictions for the quasi-linear model are obtained when the parameters estimated with X = 1.5 and 2 mm for fixed and free decoupler mounts respectively are employed. These values are comparable to the step rise amplitude of 2.38 mm in Figure 8.

Observe that the pressure oscillations in a free decoupler mount (Figure 10) decay faster than in a fixed decoupler mount (Figure 9). It is explained by the additional damped that is introduced by the decoupler switching mechanism as shown in Tables 2 and 3. This effect is even more dominant when the amplitude of oscillations has decayed to a sufficiently small value to allow the decoupler orifice to remain open for the rest of transient response (t > 0.19 sec in Figure 10). Consequently, the "decoupled" state is dominant which would attenuate the transients almost immediately. This shows that the decoupler switching mechanism is highly efficient in controlling the excitation with smaller amplitudes (X).

In Figure 10, two small "ripples" are observed in measured data, at t = 0.14 and 0.19 s, unlike the smooth responses predicted by the quasi-linear model. Both ripples correspond to quick transitions of the decoupler (from one edge to the other) due to a rapid change in the flow direction. During a short period, the inertia track is decoupled from the system and fluid flows mainly through the decoupler gap that equalizes $p_1(t)$ and $p_2(t)$. Since C_2 is very compliant such that $p_2 \approx 0$, $p_1(t)$ is almost zero in the "decoupled" state. A true nonlinear, time domain model, such as the one suggested by Adiguna *et al.* [4] and previously Kim & Singh [2], would be required to precisely capture this type of switching transients. Nevertheless, the proposed quasi-linear model predicts the overall tendency of the free decoupler mount well.

The proposed numerical and analytical models can be easily utilized for parametric or sensitivity studies. The bulge (upper chamber) stiffness k_1 and inertia track damping b_{ie} are observed to dictate the overshoot and decaying rate, respectively, of the transient responses [14].

CONCLUSION

Chief contribution of this study is to propose new estimation procedures that employ measured sinusoidal dynamic stiffness data of fixed and free decoupler mounts over the low frequency regime to characterize amplitude and frequency dependent parameters. Compared with the previously reported laboratory experiments [1-4], our estimation method requires minimal experimental effort and can be efficiently implemented by mount manufacturers or vehicle designers to quickly develop quasi-linear models and then predict transient responses with reasonable accuracy. The main limitation of the proposed method is that the predicted responses are based on the linearized approximations around operating points and as such all nonlinearities are characterized by operation-dependent parameters. Consequently, the estimated model may not truly capture significant transitions in time domain, and it should not be viewed as a "true" non-linear model. Nonetheless, better prediction would require an improved nonlinear $C_1(p_1)$ model that should incorporate the multi-staged stiffness characteristics [14]. Based on the material presented in this article, an interactive software has been developed by the authors that can be used to characterize and examine practical mounts. Finally, it is desirable to incorporate the quasi-linear and nonlinear formulations into large scale finite element or multi-body dynamic models of vehicles for system response or component allocation studies.

ACKNOWLEDGMENTS

We acknowledge the experimental efforts of M. Tiwari and J. Sorenson from 1999 to 2002. Those studies were financially supported by the Ford Motor Company.

REFERENCES

1. M. Tiwari, H. Adiguna and R. Singh, "Experimental Characterization of a Nonlinear Hydraulic Engine Mount", Noise Control Eng. J. 51(1), 36-49 (2003).
2. G. Kim and R. Singh, "Study of Passive and Adaptive Hydraulic Engine Mount Systems with Emphasis on Nonlinear Characteristics", J. Sound Vib. 179, 427-453 (1995).
3. A. Geisberger, A. Khajepour and F. Golnaraghi, "Non-linear modeling of hydraulic mounts: theory and experiment", J. Sound Vib. 249, 371-397 (2002).
4. H. Adiguna, M. Tiwari and R. Singh, "Transient Response of a Hydraulic Engine Mount", J. Sound Vib. 268, 217-248 (2003).
5. R. Singh, G. Kim and P. V. Ravindra, "Linear analysis of automotive hydro-mechanical mount with emphasis on decoupler characteristics", J. Sound Vib. 158, 219-243 (1992).
6. *Acoustics and vibration - Laboratory measurement of vibro-acoustic transfer properties of resilient elements*, International Standard ISO 10846: 1997 (International Organization for Standardization, Geneva, Switzerland, 1997).
7. MTS Elastomer test system 831.50, 1000 Hz, http://www.mts.com.
8. Matlab version 6.5, The MathWorks, Inc. (2002).
9. J. H. Lee, M. S. Bae and K. J. Kim, "Limitations of Mechanical Model With Lumped Mass in Representing Dynamic Characteristics of Hydraulic Mount", SAE Paper 2003-01-1466 (2003).
10. M. Sugino and E. Abe, "Optimum Application for Hydro-elastic Engine Mount", SAE Paper 861412 (1986).
11. E. O. Doebelin, System Dynamics: Modeling, Analysis, Simulation, Design, Marcel Dekker, Inc. (1998).

12. T. Jeong and R. Singh, “Inclusion of Measured Frequency-and Amplitude-Dependent Mount Properties in Vehicle or Machinery Models”, J. Sound Vib. 245, 385-415 (2001).
13. N. Tsujiuchi, T. Koizumi and K. Yamazaki. “Vibration Analysis of Engine Supported by Hydraulic Mounts”, SAE Paper 2003-01-1465 (2003).
14. S. He and R. Singh, "Transient Responses of Hydraulic Engine Mounts Using Linear and Nonlinear Models", to be submitted to J. Sound Vib., 2005.

CONTACT

Professor Rajendra Singh
Acoustics and Dynamics Laboratory
Center for Automotive Research
The Ohio State University
Email: singh.3@osu.edu
Phone: 614-292-9044
Website: www.AutoNVH.org